Plankton dynamics and mesoscale turbulence

Lecture given on 29 June 2010 by A. Provenzale

In aquatic ecosystems, primary production (the transformation of inorganic materials and light into living matter by photosynthesis) is operated mainly by small, unicellular algae that float freely in the upper layers of oceans and lakes and are collectively called *phytoplankton*, see for an illustration the phytoplankters depicted in figure 1. Since phytoplankton need light, they are confined to the water layer where solar radiation can penetrate. This region is called the "euphotic layer" and it has a maximum depth of about one hundred meters. In the ocean, this roughly corresponds to the depth of the mixed layer; thus, the environment where phytoplankton live is a highly energetic fluid region characterized by intense turbulent mixing.

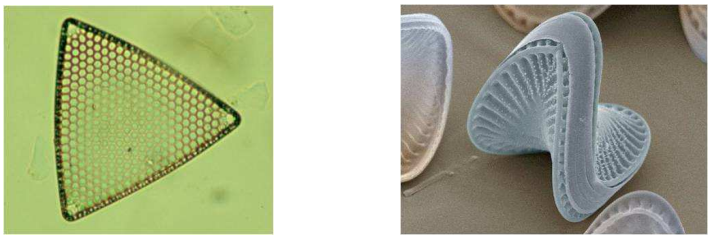

(a) (b)

Figure 1: Some examples of phytoplankton cells

Aquatic ecosystems are characterized by the essential role played by fluid dynamics. The small organisms which compose the plankton are advected by the surrounding flow and must cope with environmental currents, turbulence, and waves. And those organisms which anchor themselves to the rocks and to the bottom must prevent being wiped away by turbulent bursts. Fluid dynamics determines the motion of the individual organisms and, on a larger scale, the distribution and concentration of entire populations. Fluid dynamics and turbulence enter marine and lacustrine Ecology at all levels, and must be properly studied and understood in order to obtain a correct description of aquatic ecosystem functioning. On the other side, the transport and advection of a biologically reactive tracer, such as the plankton distribution, or of individual small living "impurities" (as we could call them) in a turbulent flow make fluid dynamics even more intriguing, opening up new problems and challenges which can stimulate the interest of the more mathematically-oriented types. In these three lectures, we shall touch upon some of these issues, with no attempt at completeness but rather barely scratching the surface of this topic.

1 Introduction

Plankton distributions in the ocean and lakes are highly inhomogeneous. One of the reasons for this inhomogeneity lies in the presence of strong horizontal advection, associated with mesoscale turbulence, coupled with the spatial inhomogeneity of the nutrient input and the nonlinear dynamics of plankton populations.

Phytoplankton are 'primary producers', which means that they take inorganic materials, such as nitrogen and carbon, and convert them into biomass via photosynthesis. The main limiting factors for phytoplankton growth are light and nutrient availability; for this reason, phytoplankton populations are confined to the upper layers of lakes and oceans, in a region known as the *euphotic* layer, see figure 1. In the ocean, nutrients are supplied by different mechanisms: (1) upwelling of deeper waters, the most crucial process as the majority of nutrients are generated by bacterial activity at depth; (2) direct bacterial regeneration of nutrients from dead biomass and excreted organic substances in the euphotic layer; and (3) dust deposition on the surface. As photosynthesis becomes less efficient when the solar radiation is too intense, and since most nutrients come from deeper waters, phytoplankton tend to live near the middle of the euphotic layer.

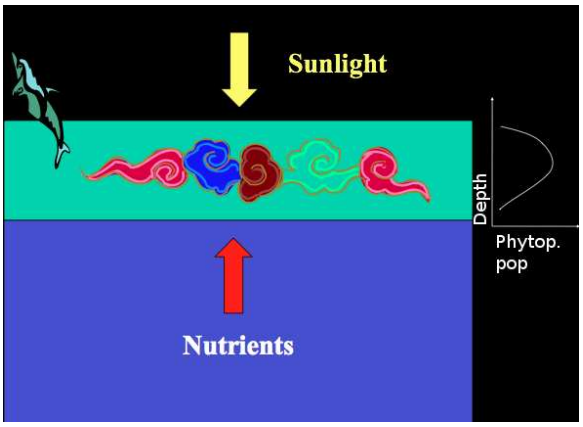

Figure 2: The structure of the upper ocean, as modeled in this lecture. Phytoplankton populations are confined to the euphotic layer (turquoise), where there is enough sunlight for photosynthesis. Nutrients are supplied mainly by upwelling of deeper waters into the euphotic layer, as the highest concentration of nutrients is at depth, where sea snow tends to settle and bacterial activity is strong. Too much sunlight is detrimental, and phytoplankton populations tend to be found near the middle of the euphotic layer.

We model meso- and large-scale interactions between fluid dynamics and biology by resorting to reaction-advection-diffusion equations. The reaction terms represent biological interactions. The advection terms here represent horizontal advection, mainly due to mesoscale circulations and flows. The diffusion terms are a parametrization of small-scale turbulence and of vertical mixing due to up- and down-welling.

2 Reaction-Diffusion Equations

Reaction-diffusion equations have the form

$$\frac{\partial \rho}{\partial t} = \mathbf{f}(\rho) + D\nabla^2 \rho, \tag{1}$$

where ρ is the concentration field of some (vector) quantity, and D is diffusivity (assumed constant and the same for all field components). The vector quantity ρ represents the concentration of different scalar fields undergoing chemical and/or biological interactions. The vector quantity $\mathbf{f}(\rho)$ represents the reactions between the various components of ρ.

In one spatial dimension and for a scalar field, this equation becomes

$$\frac{\partial \rho}{\partial t} = f(\rho) + D\frac{\partial^2 \rho}{\partial x^2}, \tag{2}$$

where x is the spatial coordinate and now ρ is a scalar.

The simplest biological example is the KISS model for plankton blooms [7, 17]. This includes a term describing Malthusian (exponential) growth and a diffusion term,

$$\frac{\partial \rho}{\partial t} = \nu\rho + D\frac{\partial^2 \rho}{\partial x^2}, \tag{3}$$

where ν is the exponential growth rate of a spatially homogeneous population. Via Fourier analysis, we can find the following expression:

$$\rho(x,t) = \frac{1}{2\pi}\int_{-\infty}^{\infty} \hat{\rho}(k)\exp(ikx)\exp[(\nu - Dk^2)t]\,dk, \tag{4}$$

and so there is instability (growth) for $k^2 < \nu/D$ (large spatial scales), while growth is restrained at small scales. This behavior leads to the presence of patchiness in the concentration field ρ with the minimum scale $2\pi(D/\nu)^{1/2}$.

To saturate the exponential growth of the homogeneous population at large times, one can include an extra term in ρ^2, and obtain the celebrated Fisher equation:

$$\frac{\partial \rho}{\partial t} = \nu\rho\left(1 - \frac{\rho}{K}\right) + D\frac{\partial^2 \rho}{\partial x^2}, \tag{5}$$

where K is a constant. We can make this equation non dimensional by rescaling space, time and the concentration field:

$$\rho \to \tilde{\rho} = \frac{\rho}{K}, \quad t \to \tilde{t} = \nu t, \quad x \to \tilde{x} = \left(\frac{\nu}{D}\right)^{1/2} x,$$

and we obtain, omitting the tilde for ease of notation,

$$\frac{\partial \rho}{\partial t} = \rho(1-\rho) + \frac{\partial^2 \rho}{\partial x^2} \tag{6}$$

where all quantities are now non-dimensional. The homogeneous version of this equation, for $\partial\rho/\partial x = 0$, is known as the logistic equation,

$$\frac{d\rho}{dt} = \rho(1-\rho) \ . \tag{7}$$

The Fisher equation admits a traveling wave solution of the form $U(z) = \rho(x - ct)$, which satisfies the following equation:

$$\frac{d^2U}{dz^2} + c\frac{dU}{dz} + U(1-U) = 0 \ , \tag{8}$$

that is,

$$\frac{dU}{dz} = V, \quad \frac{dV}{dz} = -cV - U(1-U) \tag{9}$$

where $(U, V) \equiv (U, dU/dz)$. This system of ordinary differential equations defines a two-dimensional dynamical system, which has two fixed points, namely $(U, V) = (0, 0)$ and $(U, V) = (1, 0)$. Linear stability analysis of the fixed points gives the eigenvalues $\lambda_\pm$:

$$\begin{aligned} (0,0) \quad &\rightarrow \quad \lambda_\pm = \frac{1}{2}\left[-c \pm (c^2-4)^{1/2}\right], \\ (1,0) \quad &\rightarrow \quad \lambda_\pm = \frac{1}{2}\left[-c \pm (c^2+4)^{1/2}\right], \end{aligned} \tag{10}$$

Thus, $(0, 0)$ is a stable node if $c^2 \geq 4$, and a stable focus if $c^2 < 4$; the fixed point (1,0) is a saddle. A stable focus would result in negative values of U on some trajectories near $(0, 0)$, and thus $c^2 \geq 4$ is the only physical solution. The corresponding phase-plane picture is shown in figure 3, along with a depiction of the form of the traveling wave solution (from [10]).

For general initial conditions of the form

$$\rho(x,0) = 1, \quad x < x_1; \qquad \rho(x,0) = 0, \quad x \geq x_2, \tag{11}$$

where $\rho(x_1 \leq x < x_2, 0)$ is an arbitrary function which joins 1 and 0, at large time the solution will tend to the traveling wave solution, $U(x - ct)$ with $c = 2$, see figure 4.

If we replace the second initial condition as follows

$$\rho(x,0) \approx A\exp(-ax), \quad x \rightarrow \infty, \tag{12}$$

see figure 4, then the system tends to the solution

$$\rho(x,t) \approx A\exp(-a[x-ct]), \quad x \rightarrow \infty, \tag{13}$$

where

$$c = a + \frac{1}{a} \quad \text{if} \quad 0 < a \leq 1; \qquad c = 2 \quad \text{if} \quad a > 1.$$

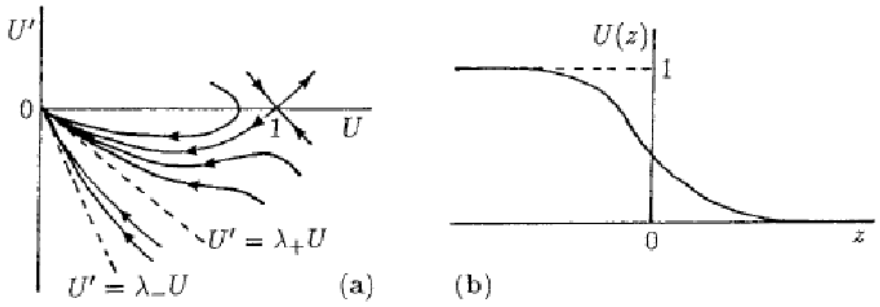

Figure 3: Panel (a) shows the phase plane trajectories for the dynamical system (9), representing the traveling wave solution of the Fisher equation (6), and panel (b) shows the traveling wave solution of equation (6), for $c \geq 2$. Both illustrations are from [10].

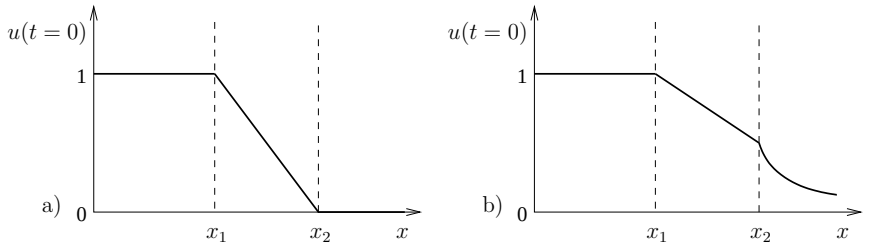

Figure 4: Qualitative description of the initial conditions which lead to a traveling wave solution, $U(x - ct)$, of the reaction-diffusion equation (6), where panel (a) shows (11) and panel (b) shows (12). The linear form of the initial conditions for $x_1 \leq x < x_2$ adopted here is for illustration purposes only.

3 Reaction-Advection-Diffusion Equations and Plankton Dynamics

In a fluid flow, reactions are affected not only by diffusion, but also by advection. In such conditions, the equations for the concentrations of reactive tracers become

$$\frac{\partial \rho}{\partial t} + \mathbf{u} \cdot \nabla \rho = \mathbf{f}(\rho) + D\nabla^2 \rho, \tag{14}$$

where $\mathbf{u}$ is the advecting flow field and D is the diffusivity (again assumed constant and the same for all components of the concentration field).

Often, the fluid velocity $\mathbf{u}$ is turbulent, and this is certainly true for the case of large and mesoscale ocean flows. Turbulent advection in aquatic ecosystems occurs on several scales. Some of these are:

Micro-scales: Between about 1 mm and a few meters, the interactions of 3-D turbulence, buoyancy and individual plankton cells are important, as will be discussed in the following lecture.

Meso- and submeso-scales: Between about 1 km and 200km, largely in the form of fronts and vortices, possibly associated with strong vertical velocities, which modulate the plankton distribution.

Large scales: Transport at ocean basin scales by large-scale gyres.

In the ocean, mesoscale advection is highly inhomogeneous, with very localized upwelling regions leading to inhomogeneous nutrient fluxes; figure 3 shows examples of mesoscale structures in the ocean dynamical properties and in the plankton distribution. In general, horizontal advection is associated with much larger velocities than vertical advection, and is responsible for transporting nutrients, phytoplankton and zooplankton as (almost) passive tracers. Advection timescales in the upper ocean are on the order of 1-7 days, which are similar to the phytoplankton and zooplankton growth timescales, which are of the order of 1-2 days and 1-2 weeks, respectively. This means that scale separation between the reaction and the advection time scales (which could allow for some simplifications) is not possible.

In keeping with the tradition of considering idealized situations, we introduce a simplified description of mesoscale turbulence in the ocean. Mesoscale ocean flows are dominated by rotation and are usually characterized by stable stratification (ignoring the localized regions of intense deep convection in some polar areas and in the Gulf of Lyons). In such conditions, one of the simplest (certainly too simple) descriptions of mesoscale ocean flows is provided by quasigeostrophic turbulence in its barotropic version, and, discarding the effects of the free surface and of differential rotation (the β-plane effect), by the formulation known as two-dimensional (2D) turbulence. Of course, this flow model cannot be taken as a true representation of mesoscale ocean flows but rather as an idealized picture that has some of the properties of the real flow (for example, the presence of intense coherent vortices).

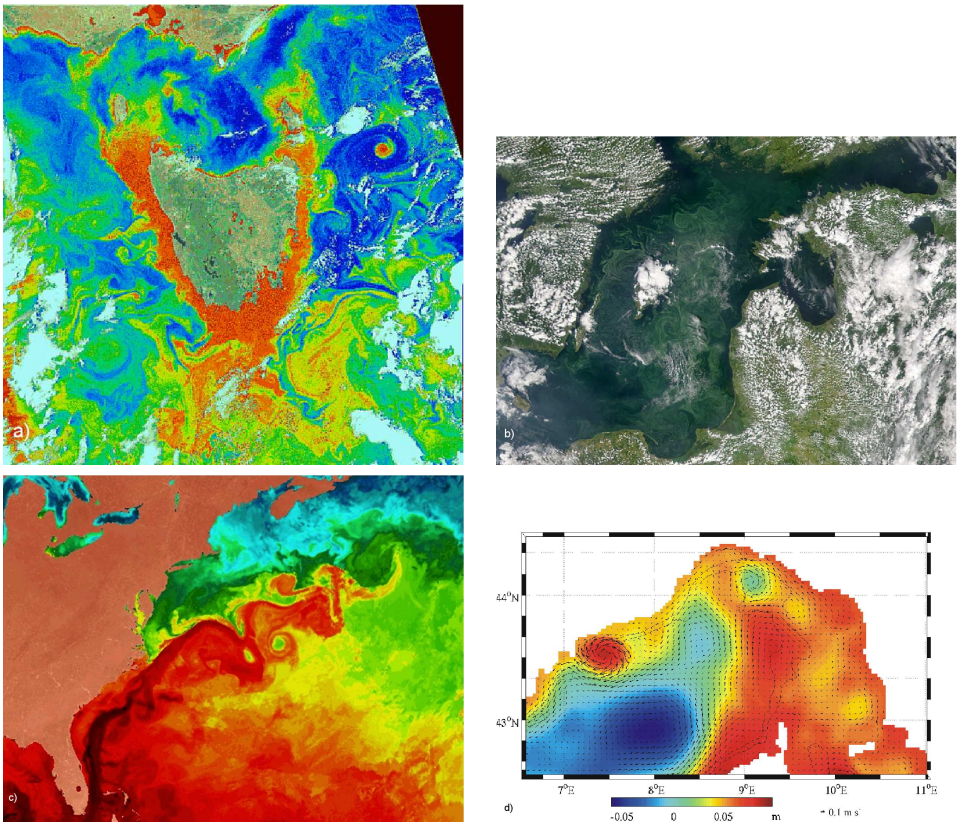

Figure 5: Examples of mesoscale structures in plankton populations and in the ocean temperature and velocity fields. Panel (a) shows the concentration of chlorophyll-a around Tasmania [11]. Panel (b) shows a phytoplankton bloom of *Nodularia spumigena* in the Baltic sea [12]. Panel (c) shows the intricate mesoscale structures in sea-surface temperature in the North Atlantic [13]. Panel (d) shows the velocity field (arrows) and the sea surface height variations (colorscale) in a patch of the Mediterranean Sea, near the coast of France and Italy [2].

The equation of motion for 2D turbulence is written as

$$\frac{\partial \zeta}{\partial t} + u\frac{\partial \zeta}{\partial x} + v\frac{\partial \zeta}{\partial y} = D + F, \tag{15}$$

where D is a (hyper)diffusion term, F is forcing, ζ is vorticity,

$$\zeta = \frac{\partial v}{\partial x} - \frac{\partial u}{\partial y} = \nabla^2 \psi \tag{16}$$

and ψ is the stream function. The horizontal velocities are given by $u = -\partial\psi/\partial y$ and $v = \partial\psi/\partial x$. Many theoretical and numerical explorations of this system have shown that a random initial vorticity field organizes into a collection of coherent vortex structures which contain most of the kinetic energy and enstrophy (squared vorticity) of the flow (see [9] for a pioneering work on this subject). Figure 6 shows an example of the vorticity field produced by numerical integration, with a pseudo-spectral code, of the forced and dissipated 2D turbulence equation (15), see [14] for further details. Here we use hypeviscosity at small scales and large-scale dissipation to balance the forcing, obtained by keeping fixed the power spectrum at a given wavenumber k_F. After a transient, the flow settles into a statistically stationary state where the average energy, enstrophy and number of coherent vortices oscillate around a constant value.

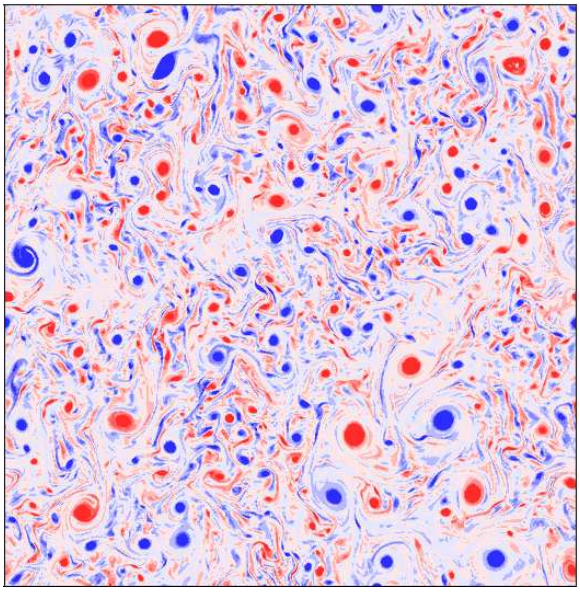

Figure 6: Vorticity field, ζ, from the numerical simulation of equation (15) with forcing and dissipation, showing the presence of intense coherent vortices.

4 The role of localized upwelling regions

Plankton growth depends on the availability of nutrients, which have to be supplied to the oceanic mixed layer to balance biological consumption. In turn, the nutrient input fluxes

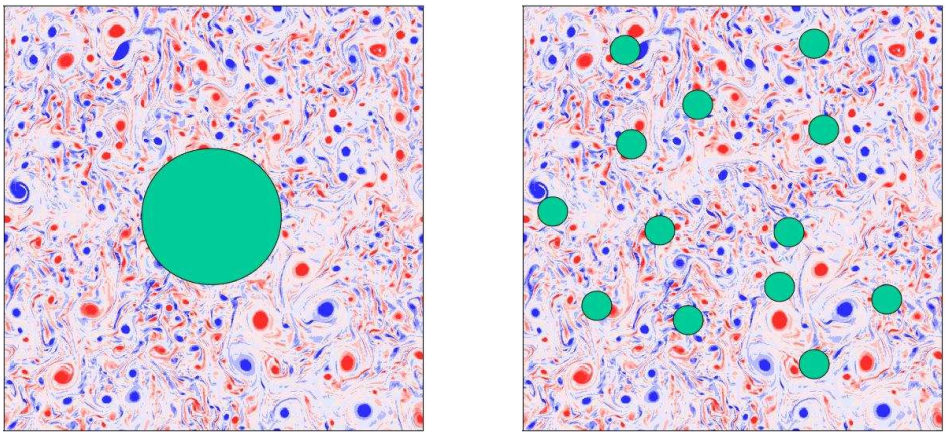

Figure 7: Green regions indicate where the intense nutrient flux takes place. The left panel refers to the case with a single region of strong upwelling (RF1), while the right panel shows a snapshot of the case where the active regions are fragmented (RFn, here n=13). The total area of the regions with strong upwelling is approximately the same in the two cases.

are affected by different physical mechanisms such as turbulent mixing, Ekman pumping, convection, transport from the boundaries etc. Such mechanisms act on a variety of scales providing spatially and temporally localized fluxes of nutrients to the biological system. Thus, it is useful to understand the behavior of a biological model in response to such inhomogeneous and intermittent forcings.

The plankton ecosystem model that is used here includes three components, that represent nutrient, N, phytoplankton, P, and zooplankton, Z (see [16] for details). The dynamics of the ecosystem is described by the reaction-advection-diffusion equations

$$\begin{aligned}
\frac{DN}{Dt} &= \Phi_N - \beta\frac{N}{k_N+N}P + \\
&\quad +\mu_N\left((1-\gamma)\frac{a\epsilon P^2}{a+\epsilon P^2}Z + \mu_P P + \mu_Z Z^2\right) + D\nabla^2 N \\
\frac{DP}{Dt} &= \beta\frac{N}{k_N+N}P - \frac{a\epsilon P^2}{a+\epsilon P^2}Z - \mu_P P + D\nabla^2 P \\
\frac{DZ}{Dt} &= \gamma\frac{a\epsilon P^2}{a+\epsilon P^2}Z - \mu_Z Z^2 + D\nabla^2 Z \ .
\end{aligned} \tag{17}$$

where $D/Dt = \partial/\partial t + u\partial/\partial x + v\partial/\partial y$.

The terms on the right hand side of the equation for the nutrient represent respectively vertical nutrient supply from deep water, nutrient consumption by phytoplankton, bacterial

regeneration of the dead organic matter into nutrients in the euphotic layer, and diffusion. Bacterial processes are here assumed to be faster than the other processes; consistently, we do not model bacterial dynamics explicitly and assume that there is a large bacterial population which adjusts instantaneously to the availability of dead matter to decompose. All variables are measured in unit of nitrogen concentration.

Phytoplankton dynamics is regulated by production, dependending on available nutrients through a Holling type-II (or Michaelis-Menten) functional response, by a Holling type III grazing by zooplankton, by linear mortality and by diffusion (see for example [8] for an overview of mathematical models in Ecology and their jargon). Finally, zooplankton grows when phytoplankton is present (γ is the assimilation efficiency of the zooplankton), and has a quadratic mortality term used to close the system and parameterize the effects of higher trophic levels.

In the nutrient equation, the term μ_N is smaller than one and represents the fact that not all biological substance is immediately available as nutrient: the fraction $(1 - \mu_N)$ is lost by sinking to deeper waters. Note, also, that nutrient enters this model by affecting the growth rate of phytoplankton. Since the formulation adopted here is two-dimensional in the horizontal and no vertical structure of the fields is allowed, vertical upwelling has to be parameterized.

Nutrient is brought to the surface from deep water by (isopycnal and diapycnal) turbulent mixing and upwelling. When these processes are sufficiently intense, it is reasonable to assume that the surface water becomes saturated in nutrients (with respect to the nutrient content in deep water) and further mixing does not change the concentration of available nutrients. Only when nutrient is removed (by phytoplankton growth and/or horizontal dispersion), vertical mixing becomes effective again. This situation can be represented by a relaxation flux, where the concentration of nutrient at the surface relaxes to a value that depends on the nutrient content in the deep reservoir. The nutrient supply can then be written in restoring form,

$$\Phi_N = -s(x, y)\ (N - N_0)\ , \tag{18}$$

where N_0 is the (constant) nutrient content in deep waters and s is the (spatially varying) relaxation rate of the nutrient, which is large in regions of strong vertical mixing and small in regions of weak vertical mixing. This form can also be interpreted as the finite-difference approximation to a vertical turbulent advective term that acts between two layers with nutrient concentration N and N_0, and it is the standard formulation used for chemostat models when the reservoir has infinite capacity.

Advection is simulated by the action of a barotropic 2D turbulent flow - an approximation to mesoscale turbulence in the ocean. We consider the case of statistically stationary 2D turbulent field, forced at the non-dimensional wavenumber $k = 40$ (that is, at a length scale which is 1/40th of the domain) and having resolution of 512^2 grid points. Assuming that the forcing scale corresponds to the typical size of an eddy, of about 25 km, then the domain size becomes 1000 km in dimensional units and the resolution is about 2 km. The

turbulent velocity field has mean eddy turnover time $T_E = 2.8$ days.

The nutrient sources are represented by a given number of randomly distributed, circular regions with fixed radius where nutrient input is stronger than average. In our simplified view, we simulate the strong nutrient flux in these patches, which we call "active regions", by a value of the relaxation rate, $s = s_a$, which is 100 times larger than the relaxation rate in the rest of the domain, which we call the "passive region" and where $s = s_p$ with $s_p \ll s_a$.

In all the numerical simulations discussed here, the turbulent velocity field is the same. What changes from one simulation to another is the spatial arrangement of the region where the flux is strong (i.e., of the "active" region). While the total area of the active region with strong upwelling is kept constant at the 12% of the domain area, the intense upwelling is respectively confined to a circular patch at the center of the domain (RF1), or to a number of small patches randomly distributed in the domain (RFn, where n indicates the number of individual patches). The two types of active regions are shown in figure 7.

To characterize the system behavior, we estimate the mean primary production, defined as $PP = \langle \beta NP/(k_n + N) \rangle$, where the angular brackets indicate average over the whole domain. Primary production can be taken as an indicator of the efficiency of the biological model to convert inorganic into organic matter.

The horizontal stirring induced by the turbulent velocity field displaces parcels of water that are rich in nutrient and planktonic life into areas of limited upwelling, where the supply is not sufficient to sustain the biological activity at the level present in the parcel. Viceversa, parcels with poor nutrient content and limited planktonic abundance can be displaced into active regions where the newly available nitrate can stimulate a plankton bloom. This effect depends on the intensity of turbulent stirring. The exchange rate of water parcels between active and inactive regions depends on the flow characteristics and on the amount of parcels that are close to the boundary areas between active and inactive regions, where there are strong gradients in the biogeochemical properties of water. The more fragmented are the upwelling regions, the larger are the boundary areas. Experiments RF1 and RFn are designed to illustrate the effects of a variation in the stirring rate on the biological activity when the size of the boundary areas with strong biogeochemical gradients is changed from small (RF1) to large (RFn), while the total upwelling area is kept constant.

The enhanced stirring induced by advection increases the mean flux from deep waters. The enhanced flux originates at active locations when a parcel of water that has low nutrient content is advected over them. To see how this happens, consider two nearby parcels: one is in a region with small nutrient upwelling and characterized by a steady-state nutrient concentration N_p^*; the other is in an active region and has a steady-state nutrient concentration N_a^*. In this configuration, the total nitrate flux associated with these two parcels of water is $\big(s_p(N_0 - N_p^*) + s_a(N_0 - N_a^*)\big)$. Suppose now that, due to advection, the two parcels switch their position: the parcel with small nutrient content gets in a strong upwelling region and viceversa. In this configuration, the vertical flux is $\big(s_p(N_0 - N_a^*) + s_a(N_0 - N_p^*)\big)$. The net variation of the nutrient flux is $(s_a - s_p)(N_a^* - N_p^*)$, which is proportional to $s_a - s_p$. This

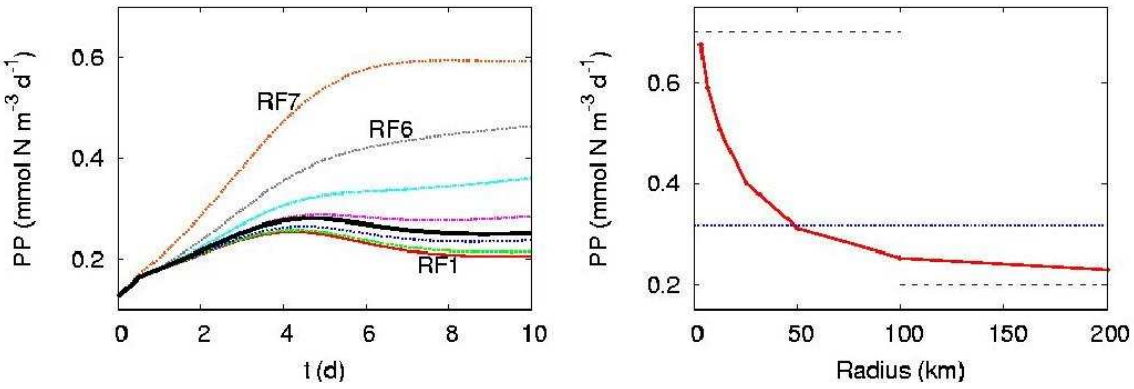

Figure 8: On the left is the time evolution of the average primary productivity. Different curves represent simulations with different number of fragmented sources (from 1 to 7). On the right is the dependence of the long-term primary productivity (that is, the value achieved after the transient of panel a) on the radius of the active regions. The total area of the regions with strong upwelling is approximately the same in the two cases.

term is positive as larger relaxation rates are found in regions with strong vertical mixing. The enhanced nutrient flux is thus due to the asymmetry in the relaxation times between the active and inactive regions. Note, also, that the exchange rate of water parcels between the two types of region directly affects the increased nutrient flux to the surface, determining larger values of the nutrient flux in the case RFn than in the case RF1.

The results reported here indicate that primary production has a strong dependence on the fragmentation level of the localized forcing, which is in turn associated with the presence and the properties of mesoscale structures. These results imply that the functioning of marine ecosystems is sgnificantly affected by the flow structure and by the distribution of the upwelling/downwelling regions, which is determined by the nature of mesoscale and submesoscale turbulence.

5 Advection over topography

As discussed above, primary productivity in the ocean depends on the availability of nutrients in the euphotic layer, which in turn depends on the presence of upwelling which brings nutrients from deeper waters.

The properties of upwelling are determined by the structure of the vertical velocities. Vertical velocities are greatly affected by the variations of topography which take place at steep continental shelves and near seamounts - areas where large abundances of plankton and fish are usually observed. In the following, we discuss the impact of a vortex propagating across a steep topographic slope on the dynamics of the plankton population [19].

The biological model is the same NPZ model used in the previous section, with the only

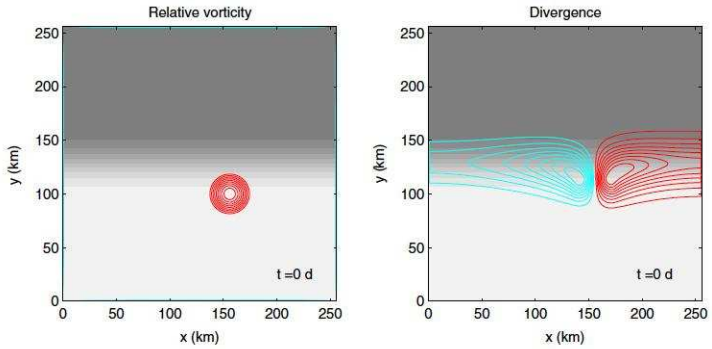

Figure 9: A cyclonic vortex on a sloping bottom topography. Vorticity is on the left; divergence on the right.

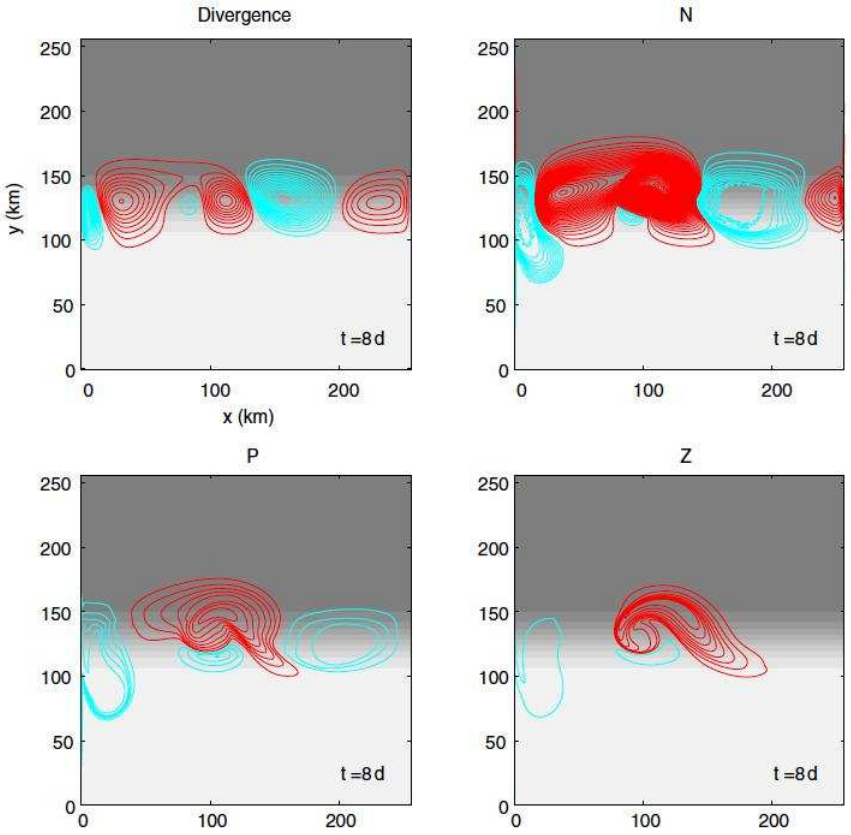

Figure 10: Contours of horizontal divergence and N, P and Z fields at t=8 days. Biological fields are plotted as deviations from their equilibrium values.

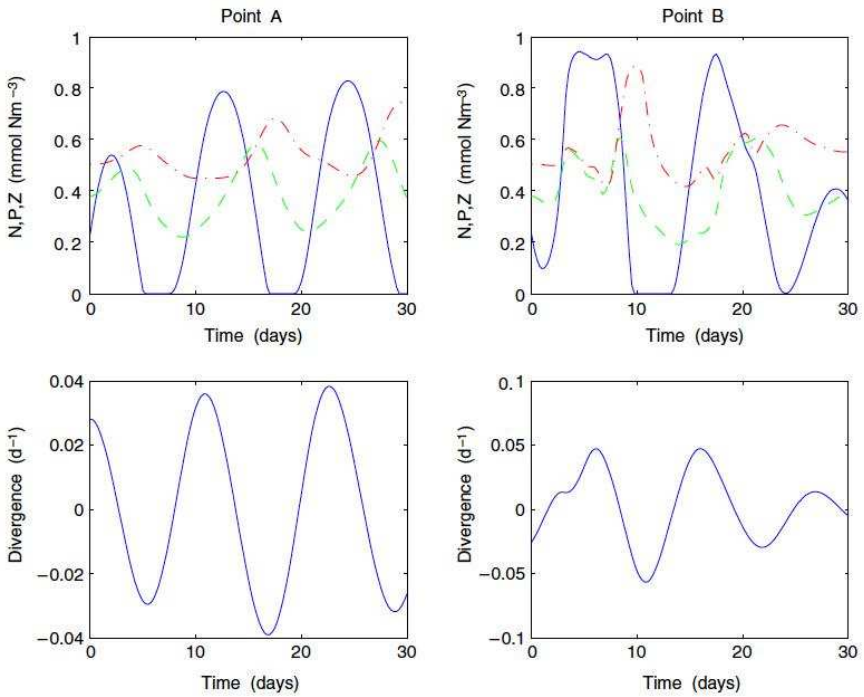

Figure 11: Time series of N,P and Z and flow divergence for two points at depth 450 meters. Solid line: N, dashed: P, dashed dotted: Z.

difference that now the vertical nutrient supply is given by the term $\Phi_N = -(s_v + s_n)(N - N_0)$, where the rate s_v is proportional to the vertical velocity of the flow and s_n represent a weak positive nutrient supply in normal conditions that allows for sustaining a non-zero population at all times. In the proximity of a vortex, $s_v \gg s_n$.

The value of s_v is determined by a Quasi-2D dynamical flow model in the presence of topography [4]. The flow is set in motion by initially placing a cyclonic vortex on the escarpment, see figure 9. The vortex is affected by the topography and it drifts leftward, according to a topographic β-effect, generating a set of propagating topographic Rossby waves associated with a pattern of vorticity, divergence and vertical velocity with alternating sign. Such motion provides an oscillating source of nutrients to the ecological model.

Figure 10 shows a snapshot of the flow divergence and of the N, P and Z fields after 8 days, when the topographic wave is travelling along the coast. The time series for N, P and Z and the flow divergence are shown in figure (11) for two points located in the sloping region at a depth of 450 m and spaced 100 km from each other. The divergence time series clearly shows an oscillatory pattern with a period of about 11 days. The amount of nutrients increases whenever there is positive divergence (that is, upward vertical velocities) and decreases if it is negative (that is, a downward velocity). As a response to this oscillating flux of nutrients, oscillatory behavior is observed also in the phyto- and zooplankton concentrations. This suggests that point measurements of ecological fields over steep slopes could reflect the characteristics of topographic waves rather than internal ecosystem dynamics; a proper interpretation of the measurements should thus take into account the properties of the Rossby waves.

6 Mesoscale Turbulence and Coexistence

As a final example, we discuss how mesoscale vortices affect species coexistence. To study this problem, we consider a system with one limiting nutrient, N, and two phytoplankton populations, P_1 and P_2 (see [1, 15] for further details). The system is assumed to be in a chemostat, i.e. there is a constantly replenishing supply of N and a constant loss of P_i:

$$\frac{DN}{Dt} = -s_0(N - N_0) - \frac{1}{\rho_1}\frac{\beta_1 N P_1}{k_1 + N} - \frac{1}{\rho_2}\frac{\beta_2 N P_2}{k_2 + N} + D\nabla^2 N, \tag{19}$$

$$\frac{DP_i}{Dt} = \frac{\beta_i N P_i}{k_i + N} - \mu_i P_i + D\nabla^2 P_i \quad i = 1, 2. \tag{20}$$

The term $-s_0(N - N_0)$ is the nutrient input, described as a relaxation to the nutrient concentration in the deep reservoir, N_0, with a rate s_0. The terms $\frac{\beta_i N P_i}{k_i + N}$ represent nutrient uptake by phytoplankton, using a Michaelis-Menten (or Monod) functional form. The constants ρ_1 and ρ_2 are used to transform phytoplankton biomass into nutrient concentration if they are described by different units (for example, nitrogen concentration for nutrient and carbon or biomass for phytoplankton). The terms $\mu_i P_i$ are natural plankton mortalities (which include possible sinking of the plankton cells) and the last terms represent diffusion. Again, the total time derivative is $D/Dt = \partial/\partial t + u\partial/\partial x + v\partial/\partial y$. No direct bacterial

regeneration term has been included.

In homogeneous conditions at equilibrium, there is no co-existence of the two plankton populations, and only the most favored species survives, as determined by the values of the different parameters. In fact, the so-called *Principle of Competitive Exclusion* [3, 5] states that if two species are too similar, they cannot coexist in equilibrium: whenever two species compete for the same resource, the most favoured will survive and the less favoured will eventually go locally extinct. By extension, at equilibrium the number of species competing on the same resources cannot be larger than the number of resources. Phytoplankton, however, seem to escape this limitation, since a large number of species that compete for the same few resources is usually observed. This phenomenon, known as the *Paradox of the Plankton*, was formulated by Hutchinson about fifty years ago [6]. Competition is avoided in many instances by partitioning space and/or time: the unfavoured species may be segregated in a spatial environment forbidden to the stronger species, or the two species might perform differently at different times. Mesoscale vortices can be one of the causes of the spatial segregation of unfavoured and favoured competitors, and the sheltering effect offered by the vortices can allow unfavoured competitors to survive for prolonged periods of time.

To study this issue, we consider system (20) with initially inhonogeneous plankton distributions and consider two alternatives for the flow advection:

1. A stochastic process representing a random walk with memory; the various 'kicks' are correlated. This flow has no coherent structures.

2. 2D turbulence, with coherent vortices.

For the stochastic process, we use a Ornstein-Uhlenbeck (Langevin) process [18], defined as:

$$\begin{aligned} dX &= u\,dt \\ dY &= v\,dt \\ du &= -\frac{u}{T_L}dt + \left(\frac{2\sigma^2}{T_L}\right) dW_x \\ dv &= -\frac{v}{T_L}dt + \left(\frac{2\sigma^2}{T_L}\right) dW_y, \end{aligned} \tag{21}$$

where T_L is the velocity autocorrelation time, σ is the standard deviation of velocities, and W_x, W_y are white-noise, Gaussian Wiener processes characterized by

$$\langle dW \rangle = 0 \tag{22}$$

$$\left\langle dW(t)dW(t') \right\rangle = \delta(t-t')dt, \tag{23}$$

such that the noise intensities at different times are not correlated. Given these assumptions, the autocorrelation of the velocity components is

$$R(\tau) = \frac{\langle u(t)u(t+\tau)\rangle}{\langle u^2(t)\rangle} = \exp(-\tau/T_L), \tag{24}$$

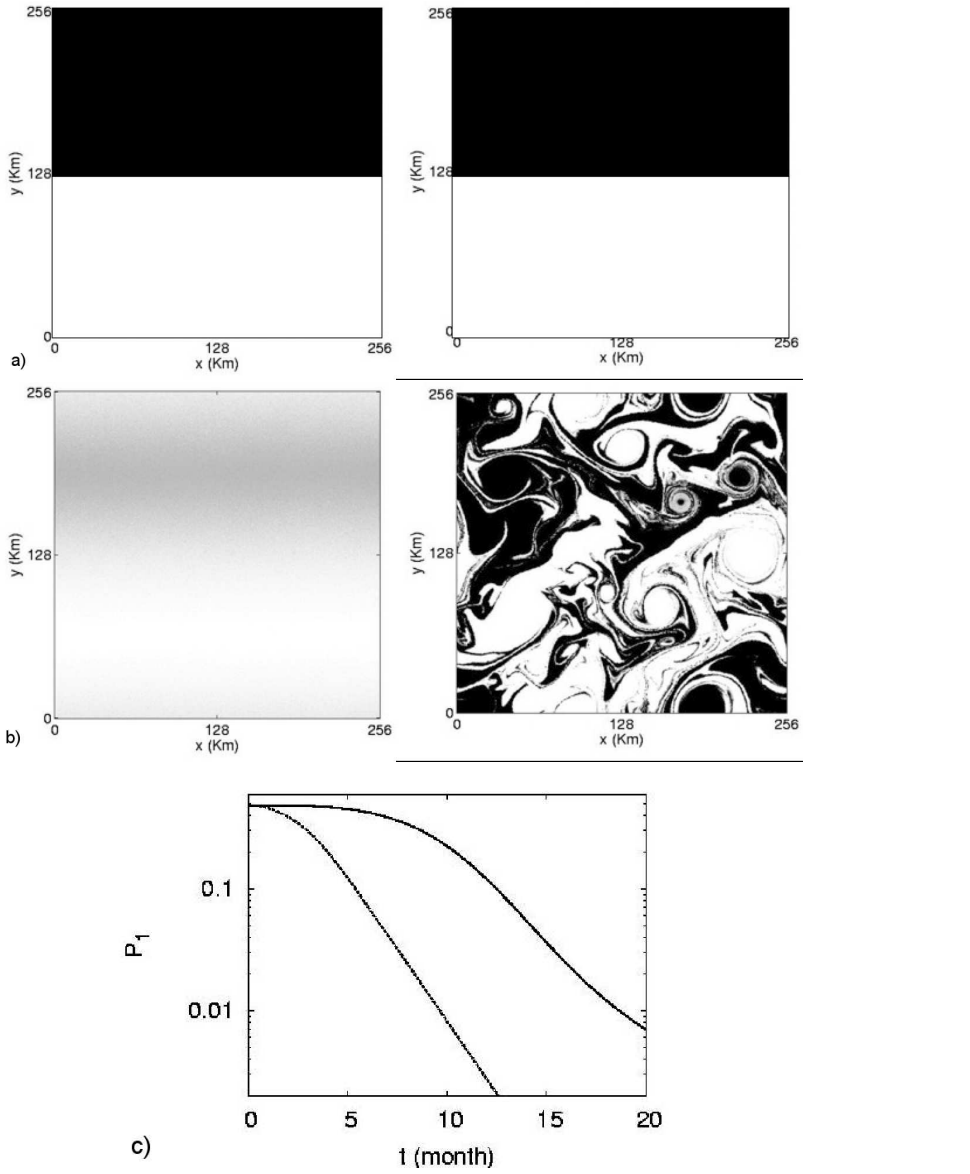

Figure 12: Panels (a) and (b) show snapshots from numerical simulations of two competing species, in white and black, described by equations (19,20), at the beginning (when they are saparate in two different regions) and at a later time, when advection has transported them across the flow domain. The left panels in both a) and b) refer to advection by the Ornstein-Uhlenbeck process described in equation (21), and the right panels refer to advection by 2D turbulence. Panel (c) shows the concentration of the less favoured population over time for the Ornstein-Uhlenbeck process (dotted line) and for 2D turbulence (solid line). The most favoured population 'wins' in both cases, but the vortices of 2D turbulence act as transport barriers and slow down the contact of the two populations and the rates of biological reactions.

such that velocities are correlated on a timescale T_L. The probability distribution of the velocity components, $p(u) = p(v)$ since the flow is statistically isotropic, is given by

$$p(u) = \frac{1}{\sqrt{2\pi}\sigma} \exp\left(-\frac{u^2}{2\sigma^2}\right). \tag{25}$$

Figure 12 shows the comparison between the plankton concentrations obtained with the two types of advecting flows, simulated in the same doubly periodic domain and with the same kinetic energy and decorrelation times, comparable with those of mesoscale turbulence in the upper layer of the ocean. The most favoured population (here represented in white) 'wins' in both cases, but it takes much longer in the case of 2D turbulence. In general, in 2D turbulence the vortices act to segregate the populations and allow the less favoured population to survive longer, providing a shelter area. In case the two populations have different fitnesses in different seasons, the presence of the vortices allows for the survival of the temporarily less fit population and for a long-term, seasonally oscillating coexistence between the two plankton populations. In conclusion, these results indicate that advection significantly affects biological reaction rates, and so it must be taken into account when studying the dynamics of marine ecosystems.

Conclusion

In this Lecture we saw that the spatial and temporal distribution of plankton at scales between a few km and a few hundred km is heavily affected by the properties of mesoscale (and submesoscale, but we did not explore it here) turbulence. If there is a message to be extracted from these examples, it is that the functioning of aquatic ecosystems is largely dependent on the fluid dynamics and that turbulence cannot be ignored.

References

[1] A. Bracco, A. Provenzale, and I. Scheuring, *Mesoscale vortices and the paradox of the plankton*, Proceedings of the Royal Society B-Biological Sciences, 267 (2000), pp. 1795–1800.

[2] E. Casella, A. Molcard, and A. Provenzale, *Mesoscale vortices in the ligurian sea and their effect on coastal upwelling processes*, J. Marine Systems, (2011).

[3] G. Gause, *The Struggle for Existence*, Hafner Press, New York, 1934.

[4] R. Grimshaw, Y. Tang, and D. Broutman, *The effect of vortex stretching on the evolution of barotropic eddies over a topographic slope*, Geophys. Astrophys. Fluid Dyn., 76 (1994), pp. 43–71.

[5] G. Hardin, *The competitive exclusion principle*, Science, 131 (1960), pp. 1292–1297.

[6] G. Hutchinson, *The paradox of the plankton*, American Naturalist, 95 (1961), pp. 137–145.

[7] H. Kierstead and L. Slobodkin, *The Size of Water Masses containing Plankton Blooms*, Journal of Marine Research, 12 (1953), pp. 141–147.

[8] M. Kot, *Elements of Mathematical Ecology*, Cambridge Un. Press, Cambridge, UK, 2001.

[9] J. McWilliams, *The emergence of isolated coherent vortices in turbulent flow*, J. Fluid Mechanics, 146 (1984), pp. 21–43.

[10] J. D. Murray, *Mathematical Biology*, Springer-Verlag, 2nd ed., 1993.

[11] NASA, November 27 1981. `http://disc.sci.gsfc.nasa.gov/oceancolor/additional/science-focus/images/tasmania_27nov81.gif`.

[12] ——, July 24 2003. `http://disc.sci.gsfc.nasa.gov/oceancolor/additional/science-focus/images/Baltic_bloom_July24_2003.jpg`.

[13] NOOA. `http://seacoos.org/Data%20Access%20and%20Mapping/currents/sst`.

[14] C. Pasquero, A. Babiano, and A. Provenzale, *Parameterization of dispersion in two-dimensional turbulence*, J. Fluid Mechanics, 439 (2001), pp. 279–303.

[15] C. Pasquero, A. Bracco, and A. Provenzale, *in "Shallow Flows", edited by G.H. Jirka and W.S.J. Uijttewaal*, Taylor and Francis, London, 2004.

[16] ——, *Impact of the spatiotemporal variability of the nutrient flux on primary productivity in the ocean*, J. Geophys. Res. - Oceans, 110 (2005), p. C07005.

[17] J. Skellam, *Random Dispersal in Theoretical Populations*, Biometrika, 38 (1951), pp. 196–218.

[18] G. E. Uhlenbeck and L. S. Ornstein, *On the theory of the brownian motion*, Phys. Rev., 36 (1930), pp. 823–841.

[19] L. Zavala Sanson and A. Provenzale, *The effects of abrupt topography on plankton dynamics*, Theoretical Population Biology, 76 (2009), pp. 258–267.